energies

MDPI

Article

Effects of Relative Roughness and Particle Size on the Interface Behavior of Concrete Suction Caisson Foundation for Offshore Wind Turbines

Wang-chun Zhang [1,2,3,4], Hao Jing [5] and Hai-lei Kou [5,*]

[1] Facility Horticulture Laboratory of University in Shandong, Weifang 262700, China; zhangwangchun@wfust.edu.cn
[2] Key Laboratory for Facility Agricultural Greenhouse Structure and Environmental Disaster Prevention and Mitigation, Weifang 262700, China
[3] Application Engineering Technology Center for High Performance Foam Concrete Development, Weifang 262700, China
[4] School of Architecture and Civil Engineering, Weifang University of Science and Technology, Weifang 262700, China
[5] College of Engineering, Ocean University of China, Qingdao 266100, China; jh1484@stu.ouc.edu.cn
* Correspondence: hlkou@ouc.edu.cn

Received: 23 September 2020; Accepted: 5 November 2020; Published: 10 November 2020

Abstract: The interface behavior between a caisson and the surrounding soil plays an important role in the installation of suction caissons as foundations for offshore wind turbines. A series of shear tests were carried out using a modified direct shear apparatus to study the interface shear behavior between sand and concrete. Sand samples with three particle size ranges (0.63–1.25 mm, 1.25–2.5 mm, 2.5–5.0 mm) and concrete plates with different relative roughness were used to explore the influence of the relative roughness parameter (R_n) and mean particle size (D_{50}) on shear behavior. The responses from the pure sand shear test are also discussed for comparison. Test results show that the higher the relative roughness (R_n), the greater the maximum shear stress (τ_{max}) appeared. The interface shear stress was weaker than that of the pure sand test. Furthermore, the interface friction angle (φ) of sand–concrete was closely related to the relative roughness of the concrete surface. Under the same conditions, the interface friction angle (φ) increased with relative roughness due to the effect of sand particles breakage and redistribution. By contrast, the effect of the mean particle size (D_{50}) on the interface friction angle (φ) was less significant. However, for the pure sand shear test, the friction angle (φ') obtained from the traditional shear test apparently increased with D_{50}, indicating that the friction angle was more affected by D_{50} in the pure sand test than in the interface shear test.

Keywords: offshore wind turbine; suction caisson; relative roughness; particle size of sand; interface behavior

1. Introduction

Suction caissons are widely used in offshore foundations for offshore wind turbines because of their great cost-saving advantages, less expensive installation equipment, shorter installation periods and being more environmentally friendly, as shown in Figure 1a [1–7]. Suction caissons are usually large, hollow, cylindrical steel or concrete structures with an upturned bucket shape. This kind of foundation structure is driven into sediments by suction and gravity, as shown in Figure 1b. The interaction behavior between the caisson and the surrounding soil has a significant impact on the installation of suction caissons [8–10]. Neglecting the interaction between the caisson and the surrounding soil or assuming a fully rough surface will cause the design or construction to be inconsistent with reality [11].

The work of many researchers highlights the importance of understanding the soil–structure interaction behavior [12–15].

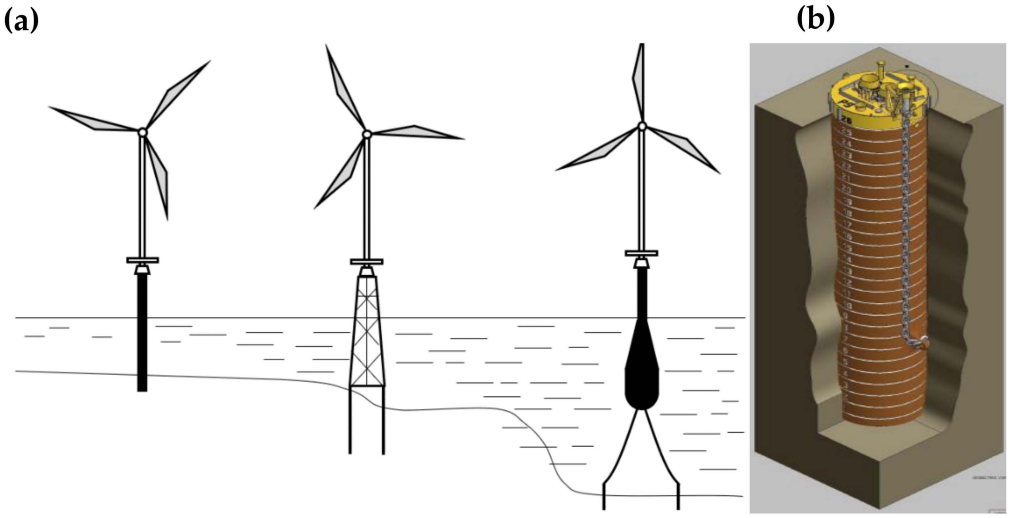

Figure 1. Typical foundation types for offshore wind turbines: (**a**) offshore wind turbines; (**b**) suction caisson foundation.

The roughness of the structure's surface, the boundary conditions, and the soil properties are the major influential factors controlling the soil–structure interaction behavior [13,16–24]. Some researchers [25–27] also used the constant normal stiffness shear test to investigate the shear behavior between sand and steel. For the soil–concrete interface, Potyondy [28] studied the skin friction of the construction materials sand, clay, cohesive granular soil and silt. Clough and Duncan [12] proposed a hyperbolic calculation model of stress displacement between soil and concrete based on a series of direct shear tests. Wernick [29] investigated the interface friction of cylindrical anchors in non-cohesive soils. Yin et al. [30] developed a contact element for soil–concrete interaction to simulate the interface deformation behavior. Modified shear apparatuses were also used to explore the shear behavior between soil and solid materials, considering surface roughness and soil type [31]. Shakir and Zhu [32] investigated the interface behavior between concrete and compacted clay by a series of interface simple shear tests. Liu et al. [33] invented a large-scale, temperature-controlled shear apparatus to investigate the shear mechanics between frozen soil and concrete. Chen et al. [34] used a large-scale shear device to investigate the effect of the relative roughness of the material surface on the interaction between red clay and concrete. Hadi et al. [35] developed a compression-to-tensile load transforming device to determine the indirect tensile strength of concrete material. At the same time, shear fracture tests and numerical study of concrete-like materials were conducted. Di et al. [36] investigated the behavior of the soil–concrete interface at different temperatures with a developed direct shear device. However, there are still few studies that explore the influence of the relative roughness of a concrete surface and the sand particle size on suction caisson behavior in offshore foundations in serviceability state.

In this study, a series of shear tests were performed with a modified shear apparatus to investigate the interaction behavior between sand and concrete. The key objective was to investigate the relationship between shear stress and horizontal displacement, and the effects of the relative roughness (R_n) of a concrete surface and mean sand particle size (D_{50}) on the shear characteristics of sand–concrete.

2. Materials and Methods

2.1. Test Sand

The sand used in this study was selected from a site near the east coast of Qingdao, China, where a proposed wind farm was being built. The grain size distribution of the collected sands is shown in

Figure 2. According to ASTM standard D6913/D6913M-17 [37], the collected sand is defined as coarse sand. The prepared sand samples were in a loose state with a void ratio of 0.85. The roundness and the sphericity were 0.49 and 0.65, respectively. As illustrated in Figure 3, sand samples of three different particle size ranges (i.e., 0.63–1.25 mm, 1.25–2.50 mm, and 2.50–5.00 mm) were prepared with the aim of exploring the influence of mean particle size (D_{50}) on the interface behavior. The physical properties of sand samples were obtained according to ASTM D422-63 [38], ASTM D558-11 [39], and ASTM D 854-14 [40], as shown in Table 1. Before the test, the sand samples were dried in a drying box for 24 h and then prepared by the screening method. Note that the moisture (water) content of the sand samples was not considered in this study.

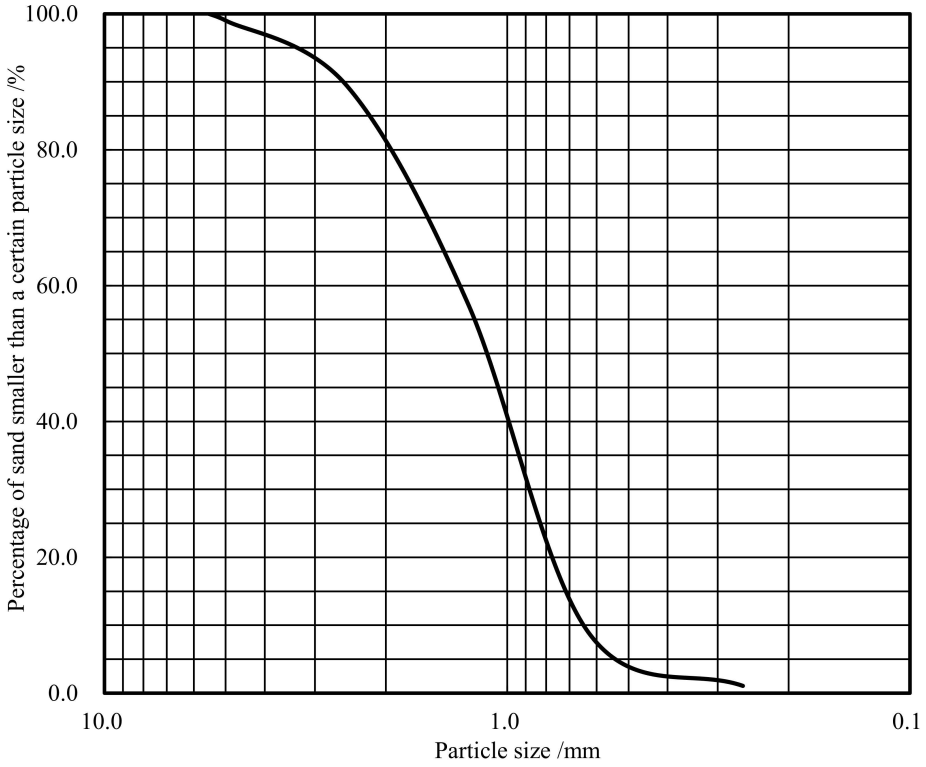

Figure 2. Grain size distribution of the sand used in this study.

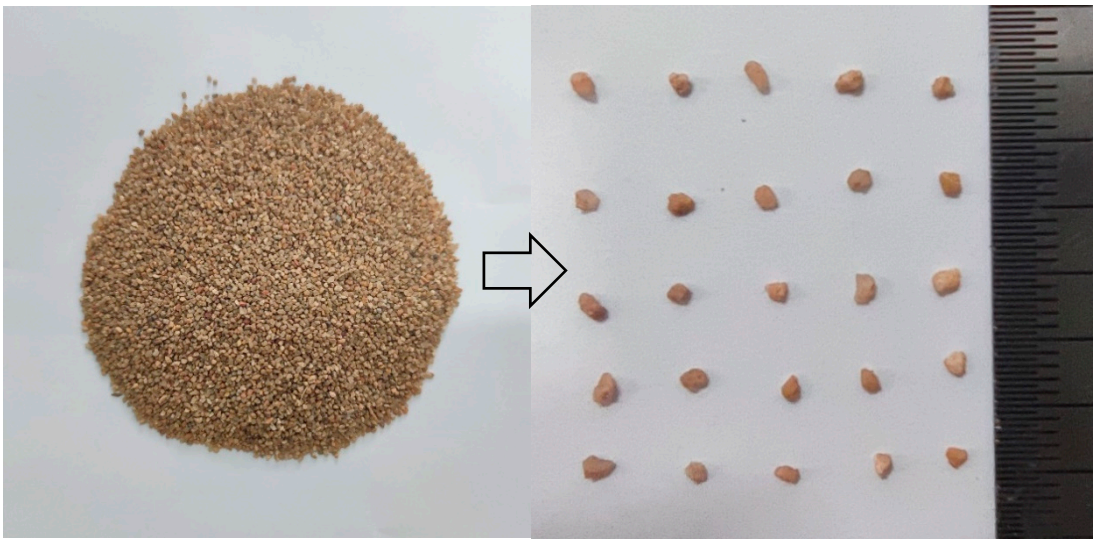

(**a**)

Figure 3. *Cont.*

(**b**)

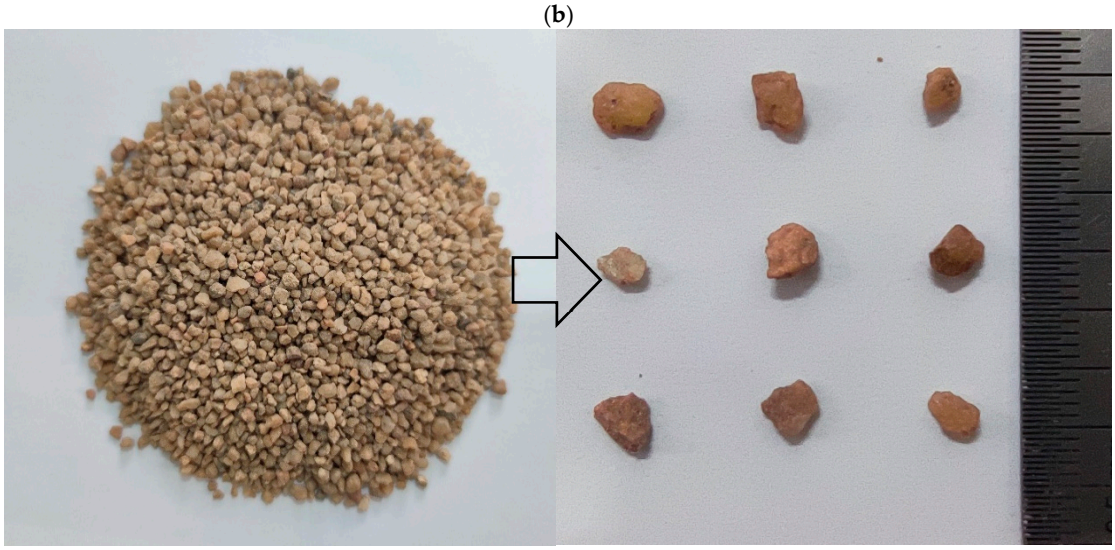

(**c**)

Figure 3. Soil samples with three ranges of particle size: (**a**) 0.63–1.25 mm sand; (**b**) 1.25–2.50 mm sand; (**c**) 2.50–5.00 mm sand.

Table 1. Basic physical properties of sand samples with different particle size ranges.

Particle Size Range (mm)	Mean Particle Size (D_{50}) (mm)	Specific Gravity (G_s)	Relative Density (D_r) (%)	Maximum Dry Density (ρ_{dmax}) (g/cm^3)	Minimum Dry Density (ρ_{dmin}) (g/cm^3)
0.63–1.25	0.71	2.65	51.39	1.67	1.37
1.25–2.50	1.43	2.65	51.39	1.69	1.39
2.50–5.00	3.50	2.67	51.39	1.73	1.45

2.2. Concrete Plates

The concrete plates were cast with C_{30} concrete and the elasticity modulus was 3.0×10^4 N/mm^2. The size of the concrete plates was 100 mm (length) × 100 mm (width) × 20 mm (thickness). Three degrees of roughness were designed for the plate surface that interacts with the sand, with the surface grooved along the length of the plate as illustrated in Figure 4. Zero, seven, and nine grooves were fabricated in parallel, respectively, to form different roughness. The cross section of the groove was an isosceles triangle with the base and the height equal to 1.0 mm. The concrete plates with different roughness were placed in the lower shear box in the test (see Figure 5). Note that this method of etching grooves on steel plates is inconsistent with reality. The actual roughness of a concrete surface should be evaluated

by a profilometer. In this study, the focus was to investigate the effect of surface roughness on the concrete–sand interface behavior, so the profilometer test was not used. The surface roughness of a structure can be evaluated by several surface roughness assessment methods, such as the sand-pouring method, silica powder clamping method, stylus profilometer method, roughness apparatus method, fractal dimension method, and unveiled coarse grain ratio method. According to Chen's study [34], the sand-pouring method, stylus touching method, and roughness apparatus method follow the same mechanism. The sand-pouring method is straightforward and convenient to use, but it ignores basic characteristics including the large smooth areas, the depth of individual grooves and regular groove layout, resulting in greater roughness. The silica powder clamping method, fractal dimension method and unveiled coarse grain ratio method are not suitable for evaluating a concrete surface with regular roughness. By considering those features of a surface of regular roughness, a modified poured-sand method was proposed by Chen et al. [34] as follow:

$$d_s = (d_{max}/d_{avg})\,(1 + k^3)\,(v_s/S) \quad (1)$$

$$k = n_g/(n_c + n_g) \quad (2)$$

where d_s is the poured sand depth; d_{max} is the shear slip thickness on the interface; d_{avg} is the average depth of the designed grooves; k is a modified parameter considering the regular layout; v_s is the volume of poured sand; S is the area of poured sand; n_g is the number of smooth zones; and n_c is the number of grooves. In this study, the surface roughness of concrete plates was evaluated using the modified poured-sand method. The calculated relative roughness (R_n) of the sand–concrete interface with zero, seven, and nine grooves was 0, 0.073, and 0.109, respectively. It was simply assumed that the surface of the concrete plate with $R_n = 0$ and the parts with no grooves were completely smooth, which was not the same as the method defined by Uesugi et al. (1986) [17].

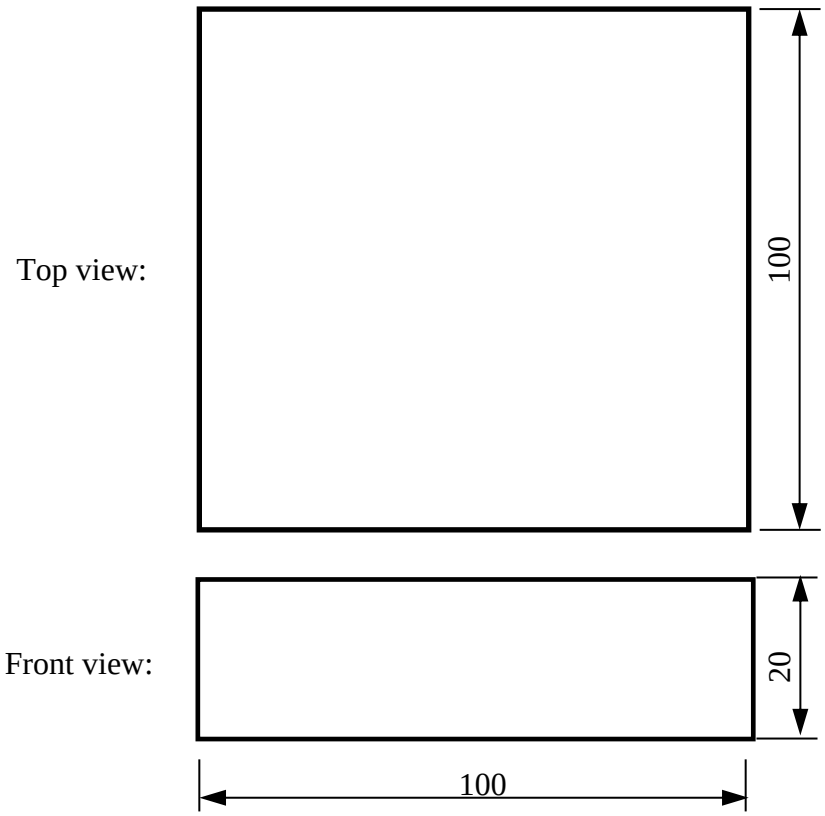

(**a**)

Figure 4. *Cont.*

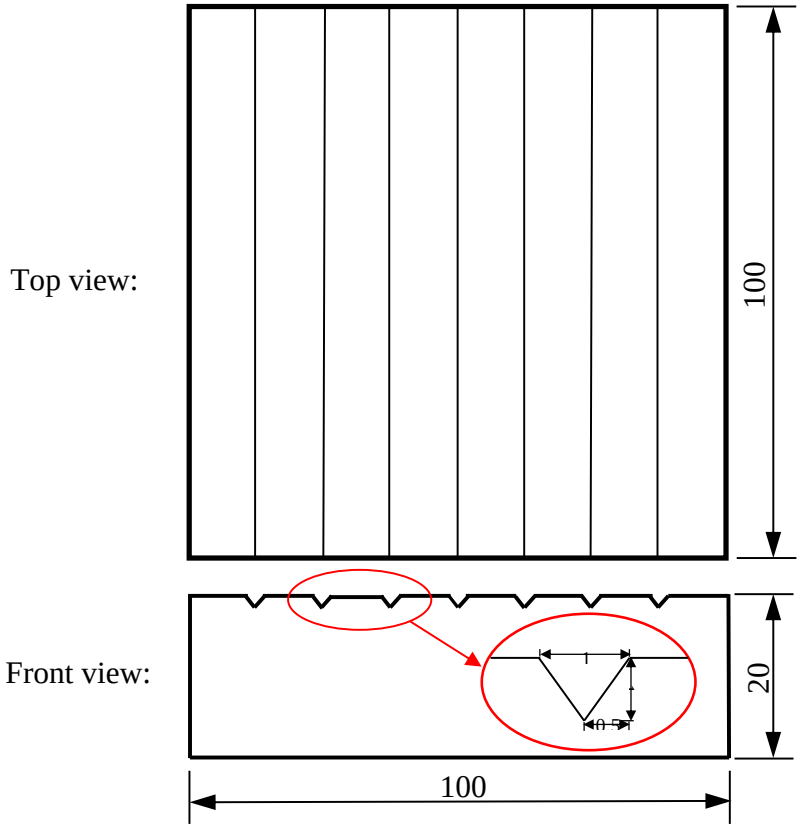

(**b**)

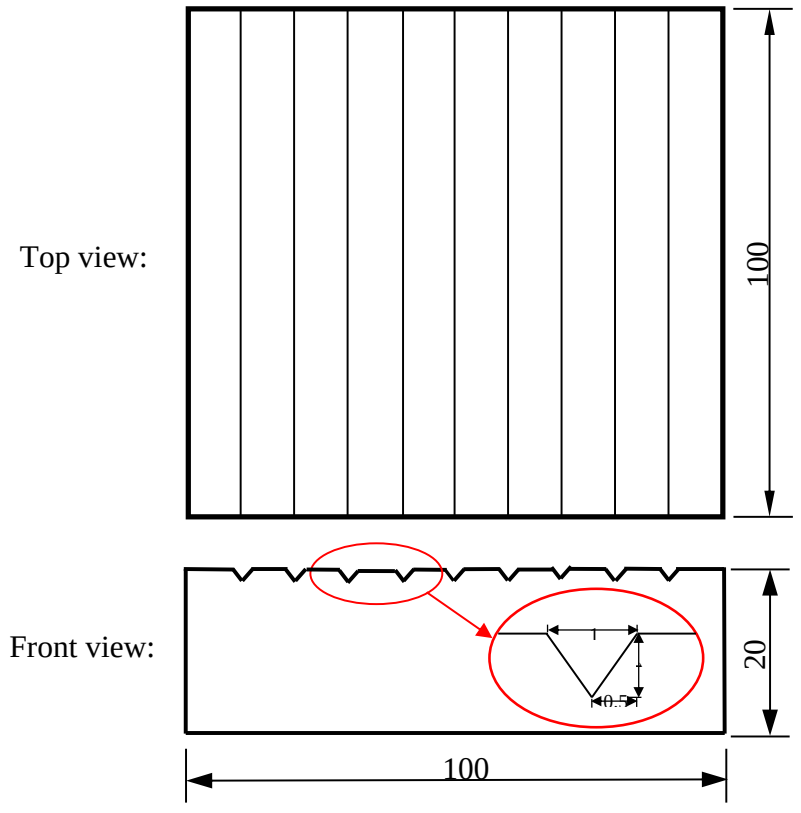

(**c**)

Figure 4. The roughness design for the concrete plate surface (unit: mm): (**a**) zero grooves; (**b**) seven grooves; (**c**) nine grooves.

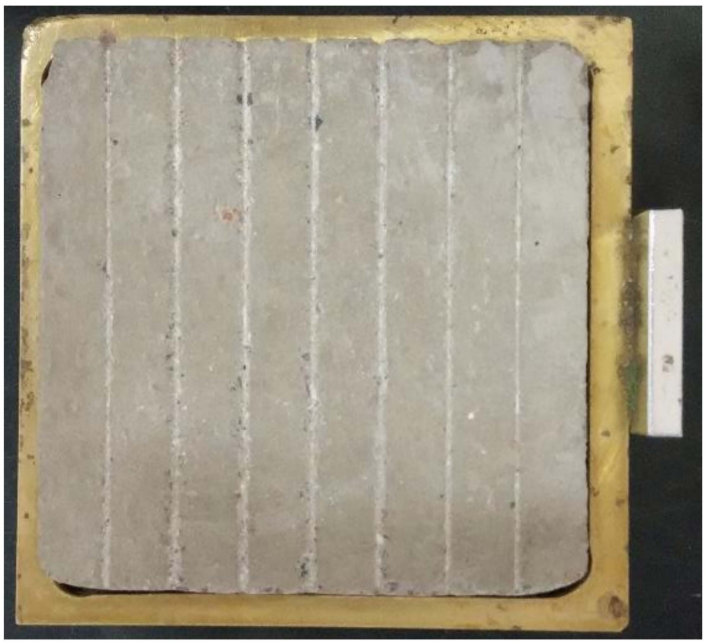

(**a**)

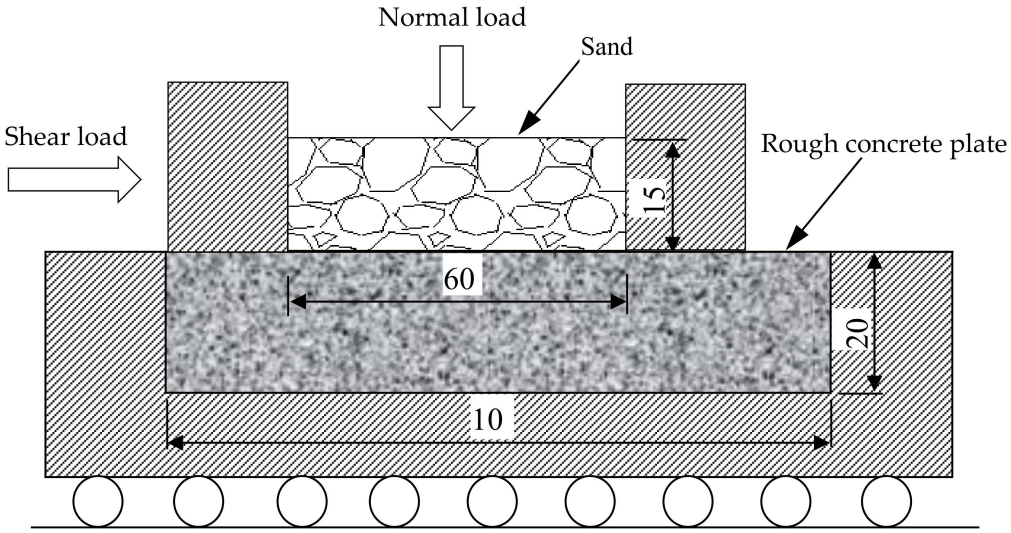

(**b**)

Figure 5. Modified test apparatus (unit: mm): (**a**) modified lower shear box; (**b**) schematic diagram of sand–concrete interface test.

2.3. Testing Method

The tests were conducted using a modified shear apparatus, as shown in Figure 5. The upper part of the shear apparatus is a hollow cylinder with 60 mm in diameter and 15 mm in height. The sand samples were poured into the upper part. The lower part of the apparatus was modified with a container (100 mm in length and 100 mm in width) that holds the concrete plate (see Figure 5a). As presented in Figure 5b, the upper part of the shear apparatus was in contact with the concrete plate. However, normal stress was not applied to the contact surface between the upper part and the concrete plate. Normal stress was applied on the top of the sand sample for each combination of relative roughness and particle size range, and was varied as 50, 100, and 150 kPa according to ASTM D3080M-11 [41]. The internal shear test was also conducted using a traditional direct shear apparatus under the same normal stress.

For all tests, the shearing displacement was applied at a constant rate of 0.8 mm/min. The shear stress and the horizontal displacement were recorded using a stress ring and dial gauge. It should be noted that the vertical displacements were not measured in the tests. Furthermore, the height of the shear apparatus was 15 mm, while the particles of the coarsest sand used in this study were between 2.5 and 5.0 mm. This means that for this sand, the shear apparatus would be composed of 3 to 6 particles along its height. This was somewhat disconcerting as the shear band developed between the solid surfaces and sand had a thickness equivalent to 5 to 10 D_{50}. Thus, the results from tests on the coarsest sand may have been influenced by this scale effect.

3. Results and Discussion

3.1. Relationship between Interface Shear Stress and Displacement

The relationship between shear stress and horizontal displacement obtained from the shear tests under the normal stress of 100 kPa are shown in Figure 6. For comparison, the responses from the shear test of pure sand under the same normal stress are also included. For all tests, the shear stress gradually increased with the horizontal displacement at the beginning until it became relatively constant after a certain amount of displacement.

Compared with the maximum shear stress (τ_{max}) measured in the shear test on pure sand, the values from the interface shear test on sand–concrete were much lower. For the sand–concrete shear test with 1.25–2.50 mm particle size, the maximum shear stress (τ_{max}) in the stress–displacement curve for the relative roughness of R_n = 0 (65.524 kPa) was the lowest, which was about 80.4% of that for pure sand (81.5 kPa). The τ_{max} value for relative roughness of R_n = 0.073 (73.014 kPa) was about 89.6% of that for pure sand. Meanwhile, the τ_{max} for the relative roughness of R_n = 0.109 (76.41 kPa) was the highest, which was about 93.8% of that for pure sand. The higher the relative roughness, the more the maximum shear stress was mobilized. For tests with normal stress levels of 50 and 150 kPa, similar behaviors were observed. This phenomenon may have been caused by the redistribution and breakage of sand particles in the shear test, which is discussed in detail in the following section.

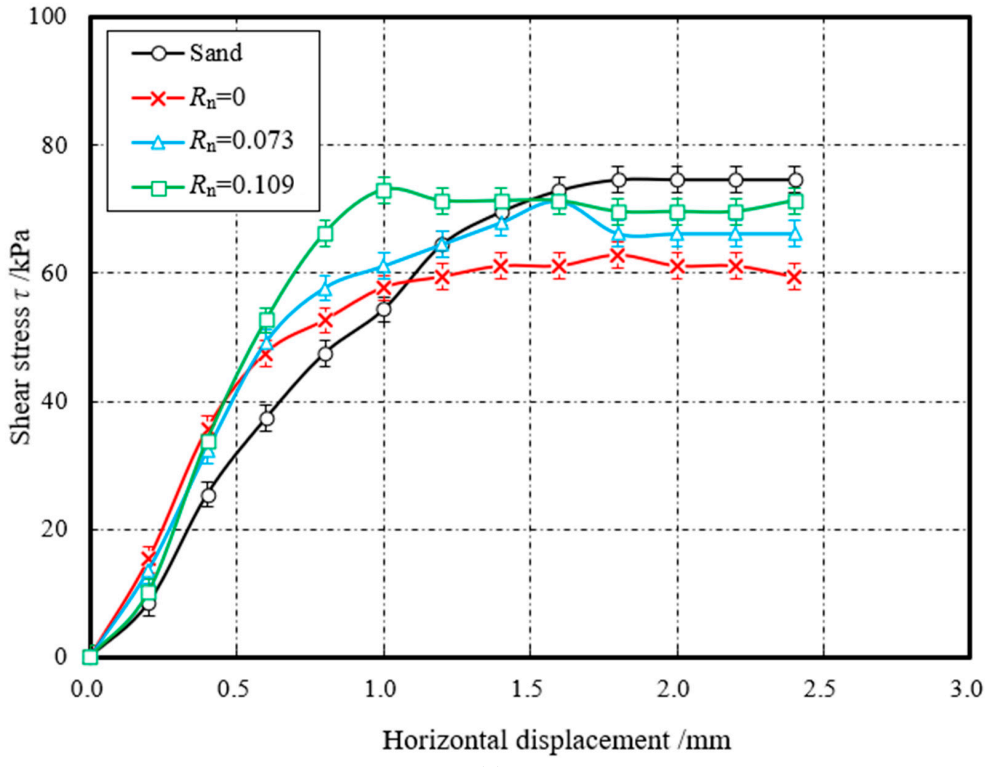

(**a**)

Figure 6. *Cont.*

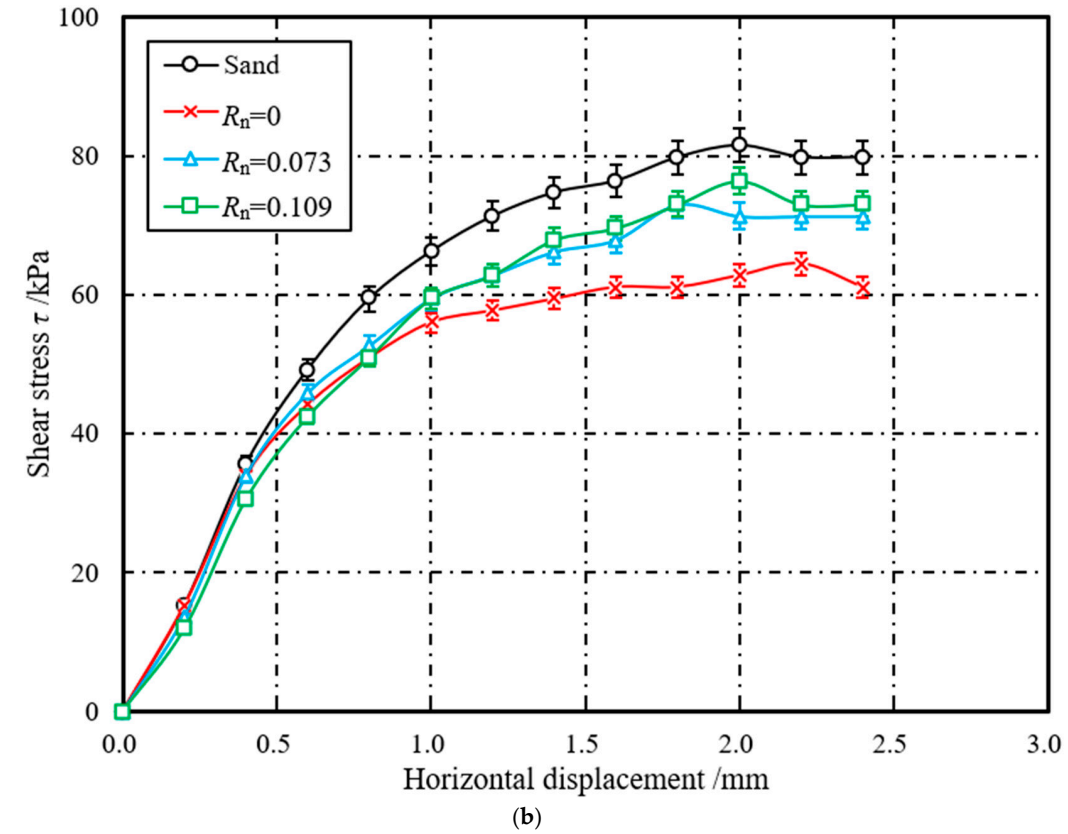

(**b**)

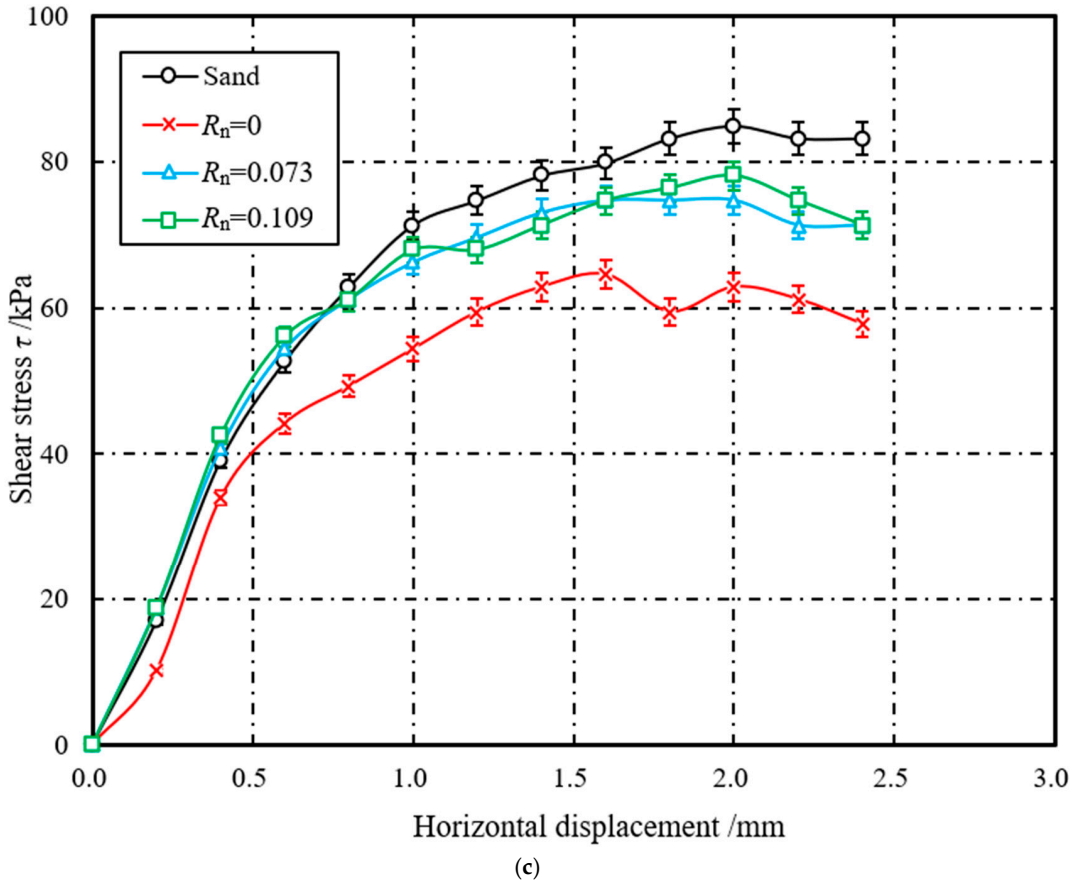

(**c**)

Figure 6. Shear stress–horizontal displacement curves for 100 kPa normal load: (**a**) 0.63–1.25 mm sand; (**b**) 1.25–2.50 mm sand; (**c**) 2.50–5.00 mm sand. Note: R_n is the relative roughness.

3.2. *Effect of Relative Roughness (R_n)*

Figure 7 shows that the maximum shear stress (τ_{max}) varies with relative roughness (R_n) under the normal stress of 50, 100, and 150 kPa for the same sand particle size ranges of 0.63–1.25 mm, 1.25–2.50 mm, and 2.50–5.00 mm, respectively. It is obvious that the maximum shear stress was greater at higher values of the normal stress. The shear strength between sand and solid material can be depicted using the Mohr–Coulomb failure criterion as

$$\tau = c + \sigma \tan\varphi \quad (3)$$

where τ is the shear stress at the interface; σ is the applied normal stress; φ is the friction angle between sand and solid material; and c is the interface adhesion. For the interface of dry sand and concrete, the interface adhesion value is considered to be zero. Based on Equation (3), the failure envelopes for the shearing between sand and concrete were obtained through fitting the data of the maximum shear stress versus the applied normal stress with a linear regression line, as shown in Figure 8. The failure envelope for pure sand is also shown in Figure 8 for comparison. For a given sand sample, the lower bound of the failure envelope was obtained from tests with $R_n = 0$, while the upper bound was from the direct shear tests of pure sand. The failure envelopes for $R_n = 0.073$ and 0.109 lie between the lower and upper bounds. This relationship indicates that the rougher interface had a stronger shear strength, but it was still weaker than that in the pure sand test.

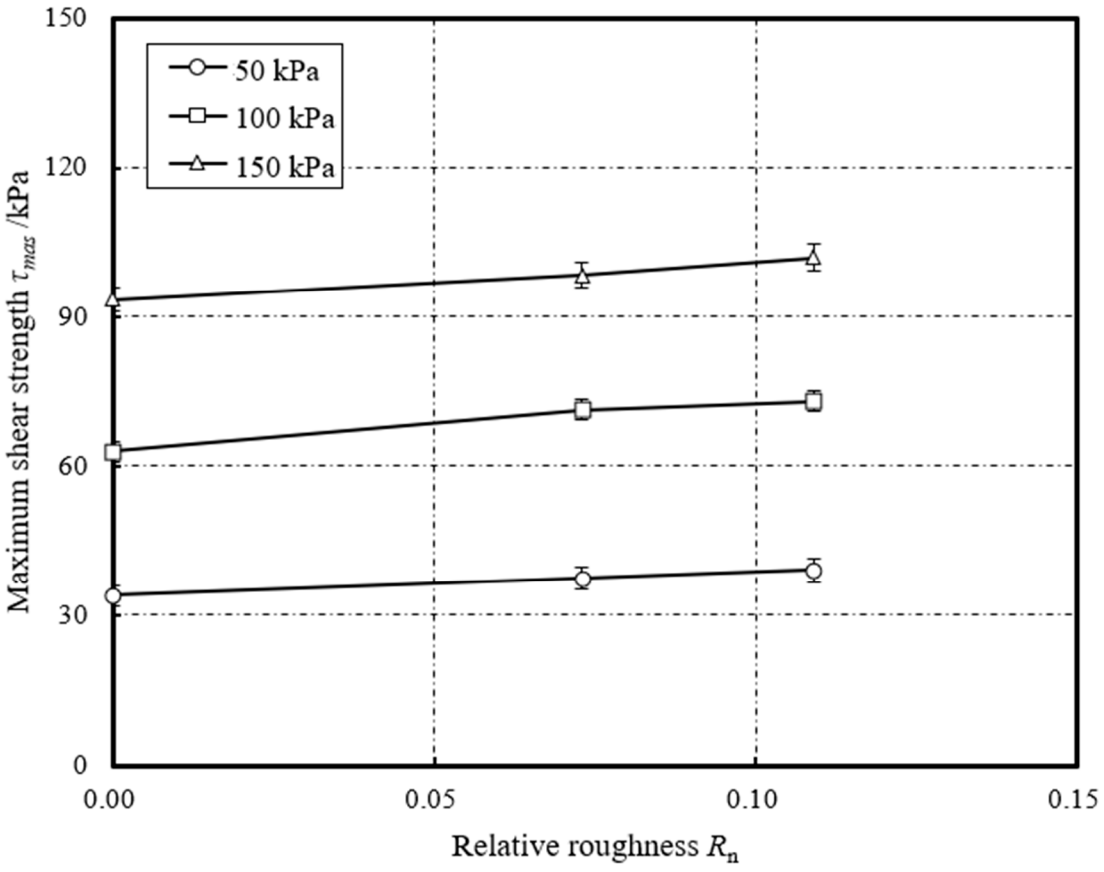

(**a**)

Figure 7. *Cont.*

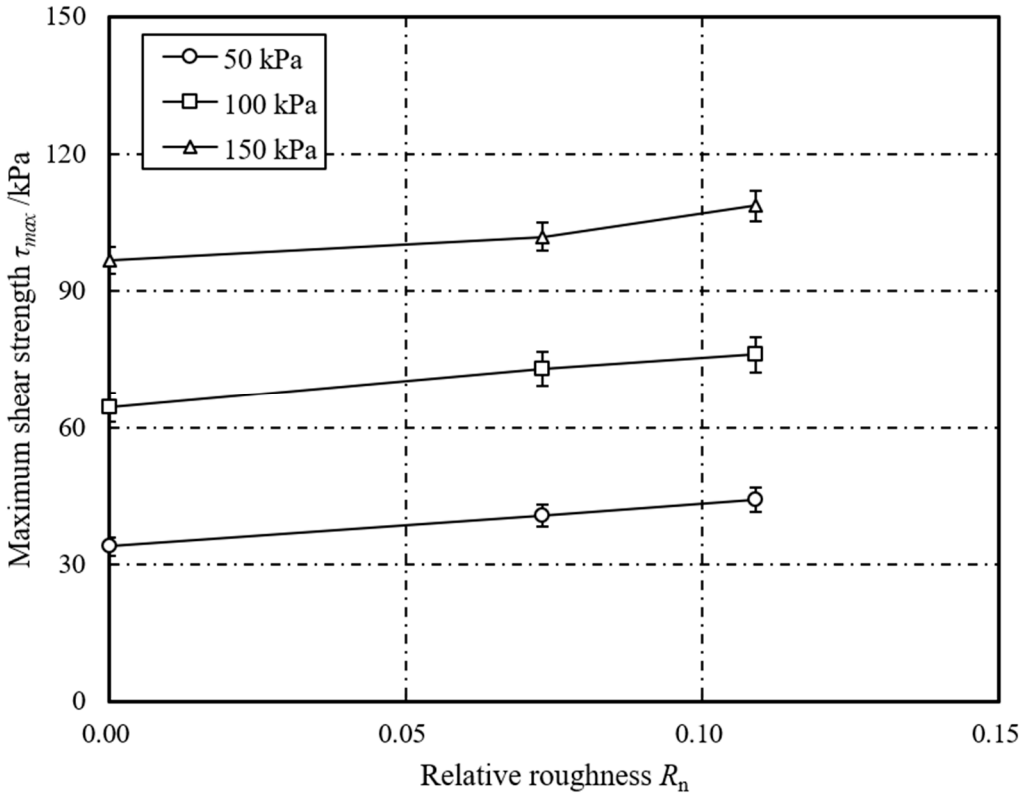

(**b**)

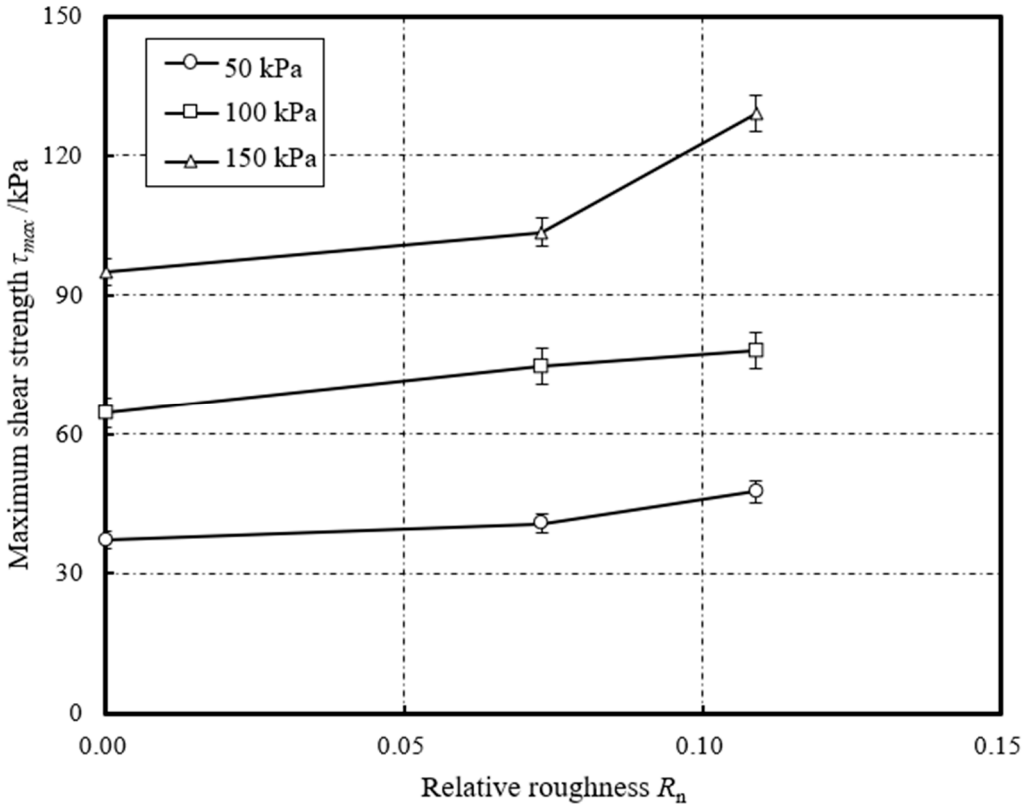

(**c**)

Figure 7. Relationships between relative roughness (R_n) and maximum shear stress (τ_{max}) under different normal stresses: (**a**) 0.63–1.25 mm sand; (**b**) 1.25–2.50 mm sand; (**c**) 2.50–5.00 mm sand.

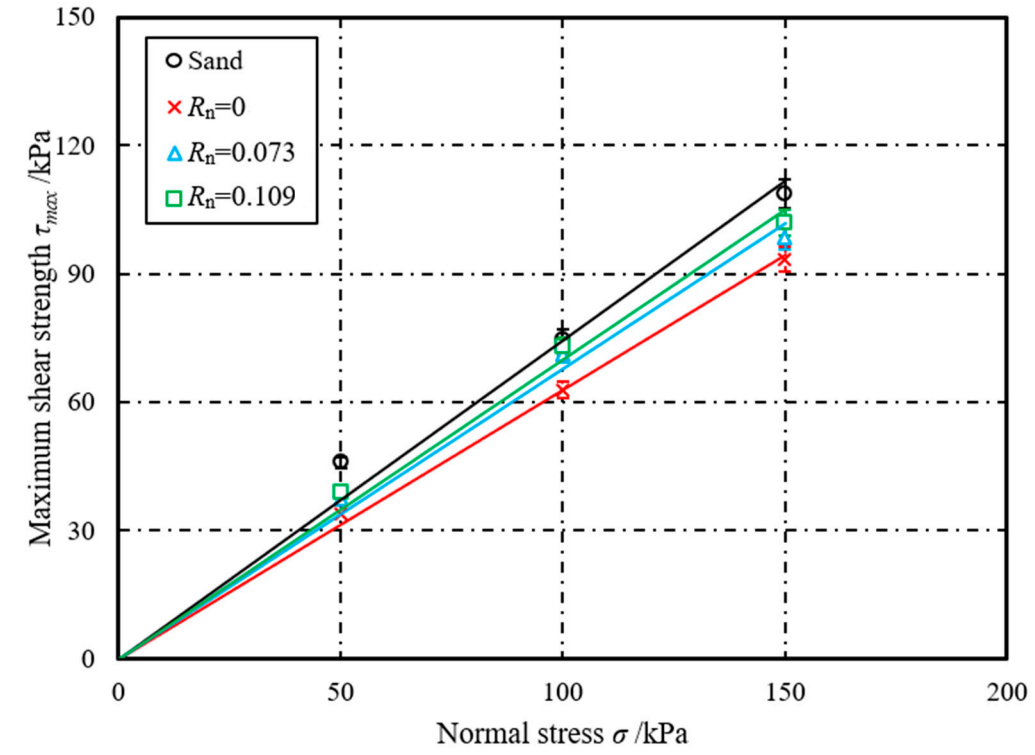

(**a**)

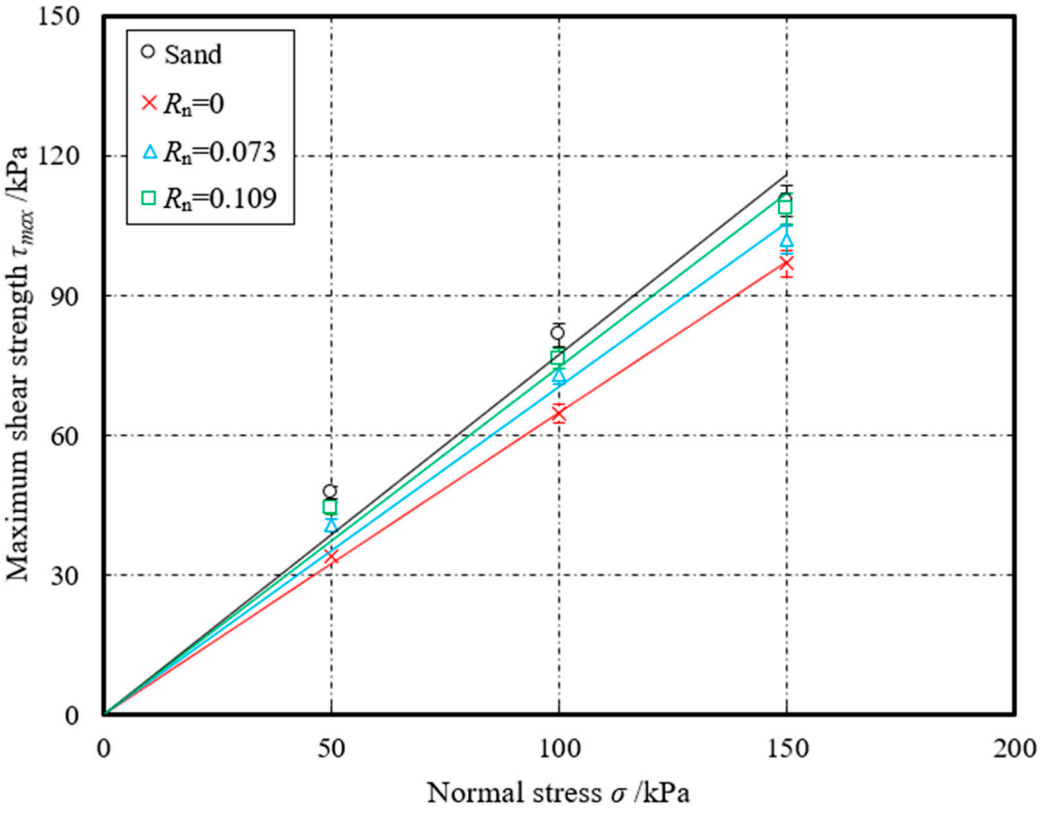

(**b**)

Figure 8. *Cont.*

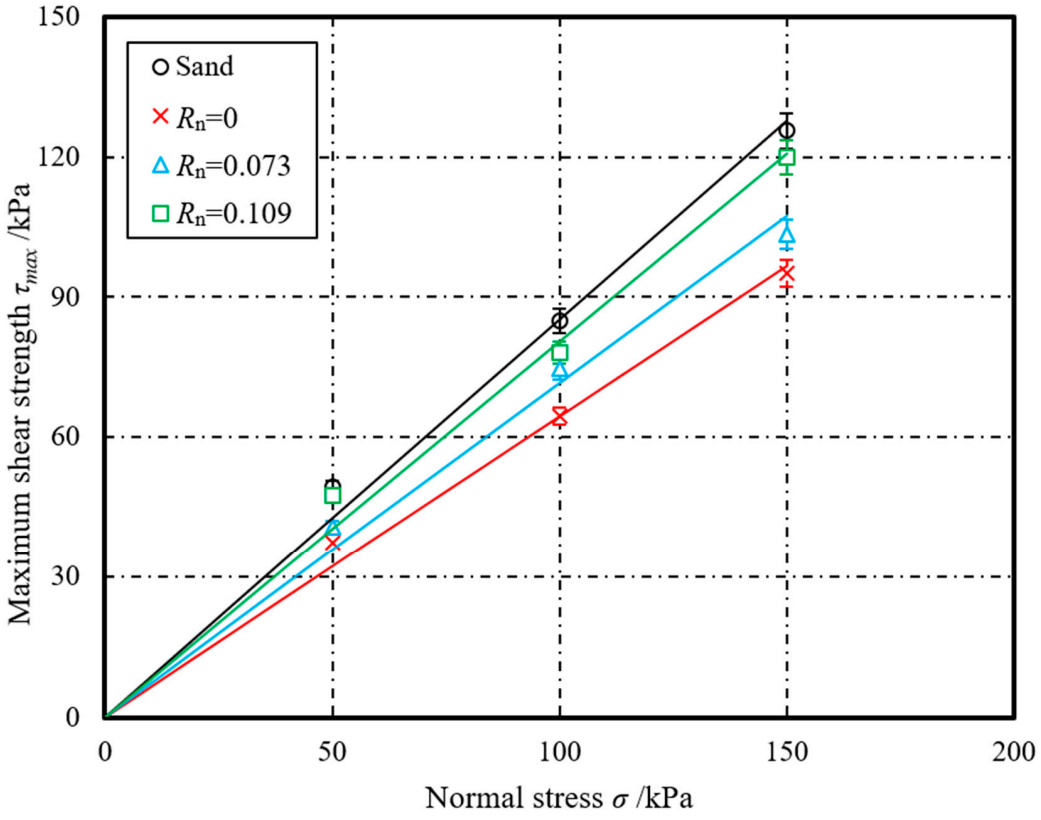

(**c**)

Figure 8. Failure envelopes of the pure sand shear tests and the interface shear tests: (**a**) 0.63–1.25 mm sand; (**b**) 1.25–2.50 mm sand; (**c**) 2.50–5.00 mm sand.

The friction angles in Equation (3) fitted from the experimental results are shown in Figure 9 as a function of the relative roughness. The corresponding values are summarized in Table 2. It is indicated that the critical state interface friction angle (φ) increased with the relative roughness for the explored values of R_n from 0 to 0.109. Taking the sand with the particle size range of 0.63–1.25 mm for an example, the friction angle (φ) between sand and concrete interface with R_n = 0 had a low value of 32.14°, while it increased to around 35.03° as R_n increased to 0.109. A similar trend was also observed for the sand samples of 1.25–2.50 mm. This can be explained by the fact that the surface of solid material with higher relative roughness can promote the redistribution process of sand particles and, thus, result in the fracture of the contact bond between sand particles in the shear test [42]. As a result, more contact area between sand and concrete in the shear test will appear and cause a greater maximum shear stress and friction angle. However, the sand with the particle size of 2.5–5.0 mm is not very representative of the performed campaign due to the scale effect.

3.3. Effect of Mean Particle Size (D_{50})

Figure 10 presents the variation of the interface friction angle (φ) with mean particle size (D_{50}) = 0.71 mm, 1.43 mm, and 3.50 mm, respectively, for particle size ranges of 0.63–1.25 mm, 1.25–2.50 mm, and 2.50–5.00 mm and for different levels of relative roughness (R_n). The friction angles (φ') of pure sand derived from the direct shear test are also included in the figure for comparison. For pure sand, it can be seen that the value of φ' increased almost linearly with D_{50}. By contrast, the impact of mean particle size (D_{50}) on the friction angle (φ) for the sand–concrete interface was less significant. Although the friction angle for different relative roughness had an average increase of 7.15% as D_{50} increased from 0.71 mm to 1.43 mm, the difference between the friction angles for D_{50} = 1.43 mm and 3.5 mm was minimal.

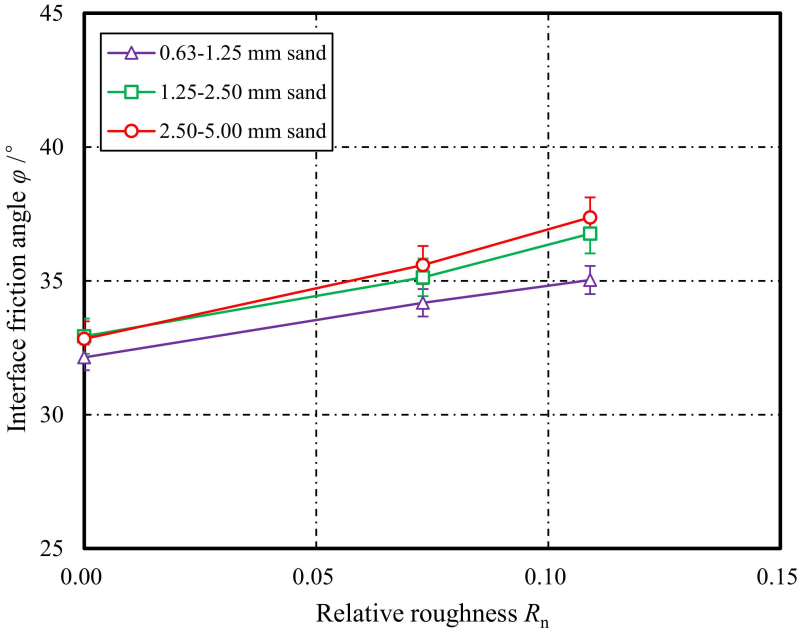

Figure 9. Variation of interface friction angle with different levels of relative roughness R_n.

Table 2. Friction angles from shear tests

Types of Shear Tests	0.63–1.25 mm	1.25–2.5 mm	2.5–5.0 mm
$R_n = 0$	32.14°	32.93°	32.83°
$R_n = 0.073$	34.18°	35.13°	35.59°
$R_n = 0.109$	35.03°	36.76°	40.17°
Pure sand	36.68°	37.73°	40.41°

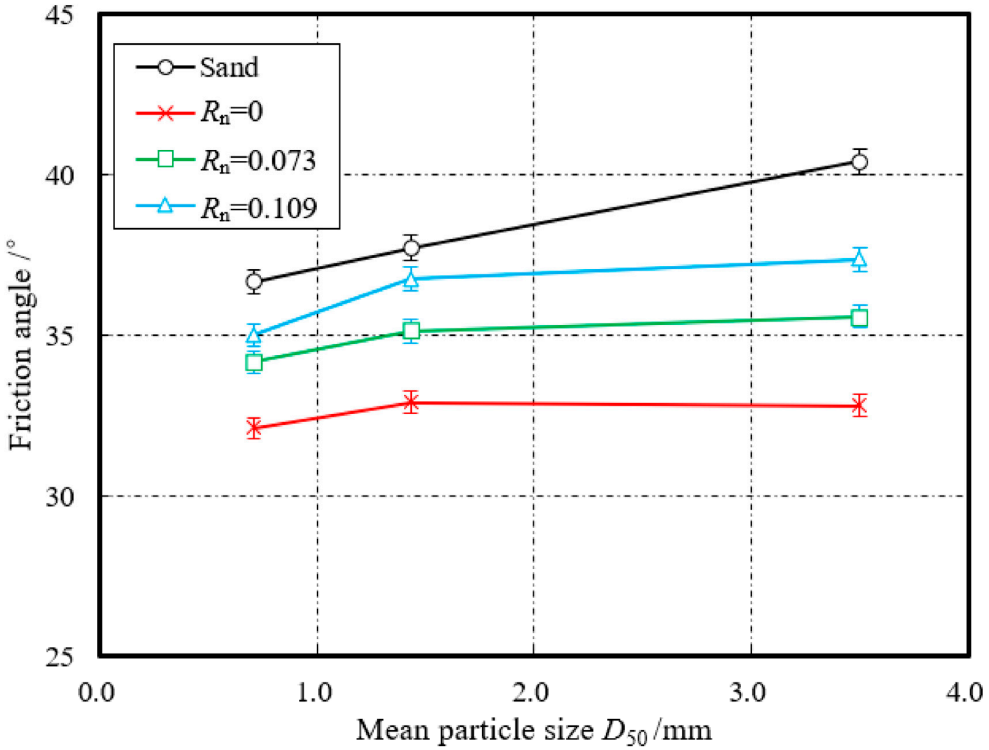

Figure 10. Relationships of mean particle size (D_{50}) and friction angle (φ) obtained from the pure sand shear tests and the interface shear tests with different levels of relative roughness (R_n).

The above phenomena can be deciphered from the perspective of particle breakage. It is well known that sand particle breakage plays an important role in shear strength [42,43]. Generally, sand with larger particles is more likely to break during shearing, as there are more flaws and defects in the particles. As shown in Figure 11, smaller particles produced by large particles can fill the void in sand samples and concrete grooves under limited pressure during the shearing process. Compared with the shearing of pure sand, particle breakage and embedded fine particles is much more significant during the interaction between sand and solid materials, due to particle collisions and rearrangements. However, the crushing was not measured in this study. Therefore, the impact of particle size on the friction angle is more significant for pure sand than for the sand–concrete interface, as large particles will eventually break into small particles due to particle breakage during the shearing process.

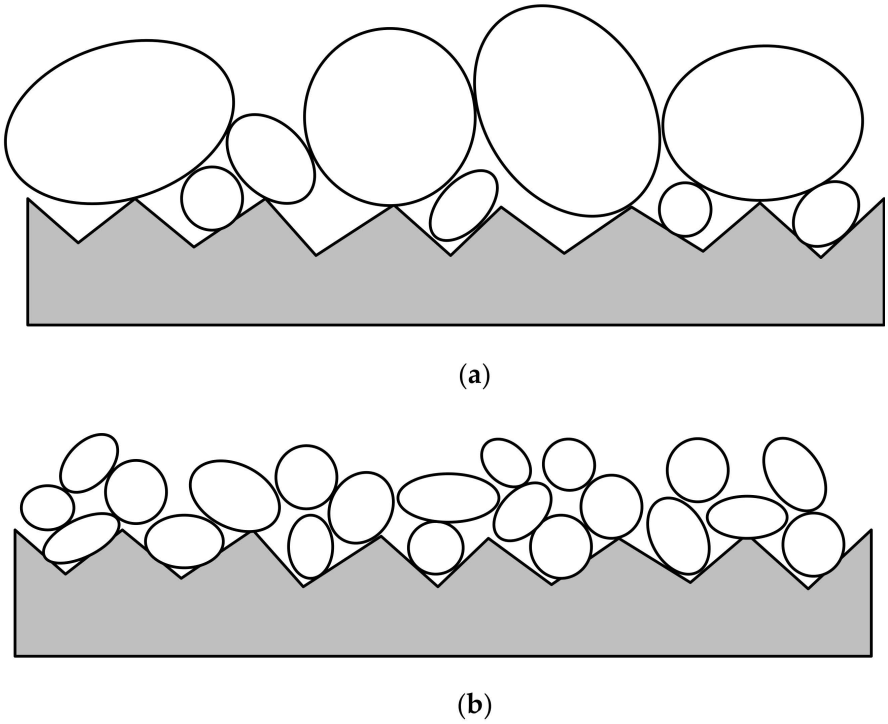

(**a**)

(**b**)

Figure 11. Sand with large particles on the interface: (**a**) before shear; (**b**) after shear.

Dietz and Ling [44] investigated the interface shear behavior between mild steel and sand under large relative displacement by a ring shear apparatus. They demonstrated the ratio of relative roughness (R_n) to mean particle size (D_{50}) (i.e., R_n/D_{50}), plotted against the interface friction angle (φ) normalized by the friction angle (φ') of pure sand (φ/φ'). This normalization brought three different trends, as shown in Figure 12. For comparison, the data obtained in this study are also illustrated in Figure 12. Note that in the study of Dietz and Ling [44], though the surface roughness was evaluated by a profilometer, the obtained roughness (R_n) was similar to that in this study. This proposed reevaluated method of relative roughness is not the same as that defined by Uesugi et al. [45]. However, this modified method was also widely used as it is straightforward and convenient. It also can be seen that the normalized data φ/φ' in this study are approximately equal to that of Dietz and Ling [44], which range from around 0.9 to 1.0. The data from Dietz and Ling [44] and Han et al. [46] are also presented in this figure for comparison. The R_n values in these two references are defined by the method of Uesign et al. [45], which was almost the same with a modified poured-sand method [35]. This indicates that the shear performance of the sand–concrete interface is similar to that of the sand–mild steel interface. This may be because this study describes post-peak shear behavior; however, these two references by Dietz and Ling [44] and Han et al. [46] describe post-peak shear behavior.

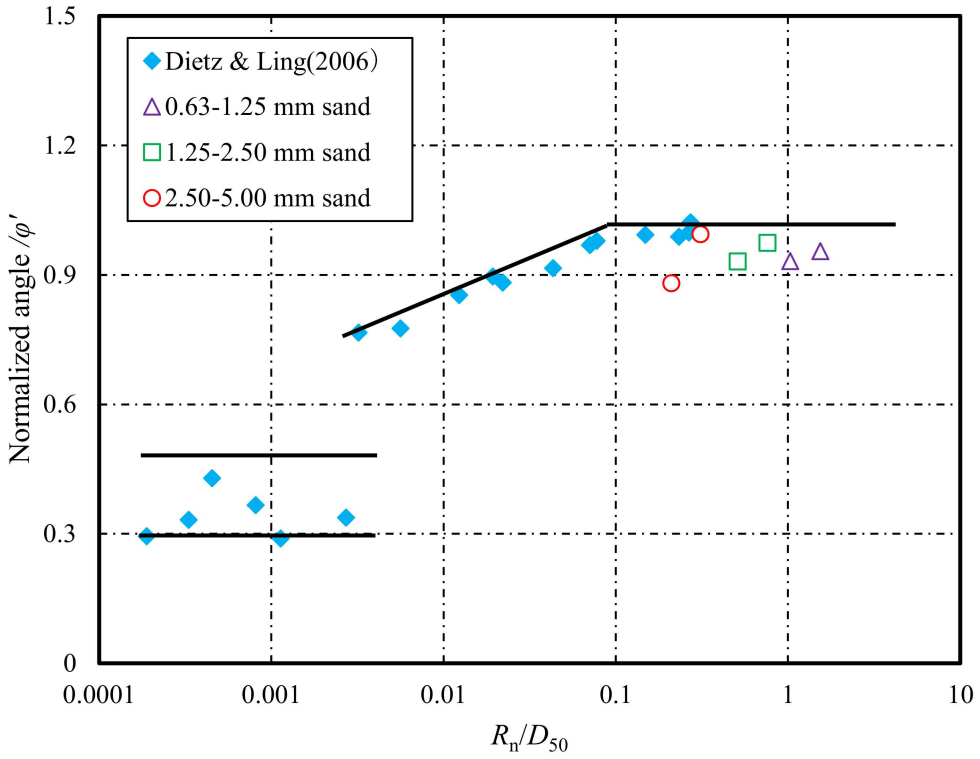

Figure 12. The relationship between R_n/D_{50} and normalized angle φ/φ'.

4. Conclusions

A series of shear tests investigating the shear behavior between sand and concrete suction caissons as foundations for offshore wind turbines were conducted. Based on the experimental results, the effects of the relative roughness of the concrete surface and particle size of sand on the shear behavior were discussed. The following major conclusions can be drawn:

1. The shear behavior between sand and concrete was affected by the levels of relative roughness (R_n). The higher the relative roughness, the larger the maximum shear stress appeared. However, the mobilized shear stress was still lower than that of the pure sand test.
2. The interface friction angle (φ) between sand and concrete was closely related to the surface relative roughness (R_n). Under the same conditions, the interface friction angle (φ) increased with the interface relative roughness (R_n), which resulted from the redistribution of sand grains and fracture of the contact bond during the shearing process.
3. The effect of mean particle size (D_{50}) on the friction angle of the sand–concrete interface was less significant than that for pure sand. This is because particle breakage and embedded fine particles were much more significant in sand–solid materials interaction.
4. The relationship between the normalized friction angle (φ/φ') and the ratio of R_n to D_{50} for the tested particle size ranges and roughness agreed well with that reported by Dietz and Ling (2006) for the sand–mild steel interface. This indicates that the shear behavior of the sand–concrete interface for the tested particle size ranges and roughness was similar to that of the sand–mild steel interface. Hence, under the premise of the tested particle size ranges and roughness, the shear behavior, considering the ratio of R_n to D_{50}, should be taken into account in practical recommendations.

Author Contributions: Conceptualization, H.-l.K.; methodology, H.J.; validation, W.-c.Z.; investigation, H.-l.K.; writing—original draft preparation, H.J.; writing—review and editing, W.-c.Z.; supervision, H.-l.K.; project administration, H.-l.K.; funding acquisition, H.-l.K. All authors have read and agreed to the published version of the manuscript.

Funding: National Natural Science Foundation of China (No. 51879246), Young Talent Program of Ocean University of China (No. 841712014) and Shandong Provincial Natural Science Foundation, China (No. ZR2019MEE056).

Acknowledgments: The authors gratefully acknowledge the financial support provided by the National Natural Science Fund of China (No. 51879246), Young Talent Program of Ocean University of China (No. 841712014) and Shandong Provincial Natural Science Foundation, China (No. ZR2019MEE056).

Conflicts of Interest: The authors declare no conflict of interest.

References

1. Andersen, K.H.; Dyvik, R.; Schroder, K.; Hansteen, O.E.; Bysveen, S. Field Tests of Anchors in Clay II: Predictions and Interpretation. *J. Geotech. Eng.* **1993**, *119*, 1532–1549. [CrossRef]
2. Hu, L.; Pu, J. Testing and modeling of soil-structure interface. *J. Geotech. Geoenviron. Eng.* **2004**, *130*, 851–860. [CrossRef]
3. Sparrevik, P. Suction pile technology and installation in deep waters. In Proceedings of the Offshore Technology Conference, Houston, TX, USA, 6–9 May 2002.
4. Randolph, M.F.; Gaudin, C.; Gourvenec, S.M.; White, D.J.; Boylan, N.; Cassidy, M.J. Recent advances in offshore geotechnics for deep water oil and gas developments. *Ocean Eng.* **2011**, *38*, 818–834. [CrossRef]
5. Barari, A.; Ibsen, L.B. Undrained response of bucket foundations to moment loading. *Appl. Ocean Res.* **2012**, *36*, 12–21. [CrossRef]
6. Ukritchon, B.; Keawsawasvong, S. Undrained pullout capacity of cylindrical suction caissons by finite element limit analysis. *Comput. Geotech.* **2016**, *80*, 301–311. [CrossRef]
7. Nielsen, S.D. Finite element modeling of the tensile capacity of suction caissons in cohesionless soil. *Appl. Ocean Res.* **2019**, *90*, 101866. [CrossRef]
8. Iskander, M.; El-Gharbawy, S.; Olson, R. Performance of suction caissons in sand and clay. *Can. Geotech. J.* **2002**, *39*, 576–584. [CrossRef]
9. Shahr-Babak, M.M.; Khanjani, M.J.; Qaderi, K. Uplift capacity prediction of suction caisson in clay using a hybrid intelligence method (GMDH-HS). *Appl. Ocean Res.* **2016**, *59*, 408–416. [CrossRef]
10. Maniar, D.R. A Computational Procedure for Simulation of Suction Caisson Behavior under Axial and Inclined Loads. Ph.D. Thesis, the University of Texas at Austin, Austin, TX, USA, 2004.
11. Stutz, H.; Masin, D.; Wuttke, F. Enhancement of a hypoplastic model for granular soil-structure interface behaviour. *Acta Geotech.* **2016**, *11*, 1249–1261. [CrossRef]
12. Clough, G.W.; Duncan, J.M. Finite element analyses of retaining wall behavior. *J. Soil Mech. Found.* **1971**, *97*, 1657–1673.
13. Martinez, A.; Frost, J.D.; Hebeler, G.L. Experimental study of shear zones formed at sand/steel interfaces in axial and torsional axisymmetric tests. *Geotech. Test. J.* **2015**, *38*, 409–426. [CrossRef]
14. Hadi, H. Simulating the crack propagation mechanism of pre-cracked concrete specimens under shear loading conditions. *Strength Mater.* **2015**, *47*, 618–632.
15. Hadi, H.; Vahab, S.; Ahmadreza, H. Suggesting a new testing device for determination of tensile strength of concrete. *Struct. Eng. Mech.* **2016**, *60*, 939–952.
16. Desai, C.S.; Drumm, E.C.; Zaman, M.M. Cyclic testing and modeling of interfaces. *J. Geotech. Eng.* **1985**, *111*, 793–815. [CrossRef]
17. Uesugi, M.; Kishida, H.; Uchikawa, Y. Frictional resistance at yield between dry sand and mild steel. *Soils Found.* **1986**, *26*, 139–149. [CrossRef]
18. Desai, C.S.; Rigby, D.B. Cyclic interface and joint shear device including pore pressure effects. *J. Geotech. Geoenviron. Eng.* **1997**, *123*, 568–579. [CrossRef]
19. Subba Rao, K.S.; Allam, M.M.; Robinson, R.G. Interfacial friction between sands and solid surfaces. *Geotech. Eng.* **1998**, *131*, 75–82. [CrossRef]
20. DeJong, J.T.; Frost, J.D.; Saussus, D.R. Measurement of relative surface roughness at particulate—Continuum interfaces. *J. Test. Eval. JTEVA* **2002**, *30*, 8–19.
21. DeJong, J.T.; Randolph, M.F.; White, D.J. Interface load transfer degradation during cyclic loading: A microscale investigation. *Soils Found.* **2003**, *43*, 81–93. [CrossRef]
22. Lashkari, A. Prediction of the shaft resistance of non-displacement piles in sand. *Int. J. Numer. Anal. Methods Geomech.* **2013**, *37*, 904–931. [CrossRef]

23. Martinez, A.; Frost, J.D. The influence of surface roughness form on the strength of sand–structure Interfaces. *Géotech. Lett.* **2017**, *7*, 104–111. [CrossRef]
24. Kou, H.; Chu, J.; Guo, W.; Zhang, M. Pile load test of jacked open-ended prestressed high-strength concrete pipe pile in clay. *Proc. Inst. Civ. Eng.-Geotech. Eng.* **2018**, *171*, 243–251. [CrossRef]
25. Hryciw, R.D.; Irsyam, M. Behavior of sand particles around rigid ribbed inclusions during shear. *Soils Found.* **1993**, *33*, 1–13. [CrossRef]
26. Porcino, D.; Fioravante, V.; Ghionna, V.N.; Pedroni, S. Interface behavior of sands from constant normal stiffness direct shear tests. *Geotech. Test. J.* **2003**, *26*, 289–301.
27. Lehane, B.M.; White, D.J. Lateral stress changes and shaft friction for model displacement piles in sand. *Can. Geotech. J.* **2005**, *42*, 1039–1052. [CrossRef]
28. Potyondy, J.G. Skin friction between various soils and construction materials. *Geotechnique* **1961**, *11*, 339–353. [CrossRef]
29. Wernick, E. Skin friction of cylindrical anchors in noncohesive soils. In Proceedings of the Symposium on Soil Reinforcing and Stabilizing Techniques, Sidney, Australia, 16–19 October 1978; pp. 201–219.
30. Yin, Z.Z.; Zhu, H.; Xu, G.H. A study of deformation in the interface between soil and concrete. *Comput. Geotech.* **1995**, *17*, 75–92.
31. Subba Rao, K.S.; Allam, M.M.; Robinson, R.G. Drained shear strength of fine-grained soil–solid surface interfaces. *Proc. Inst. Civ. Eng.-Geotech. Eng.* **2000**, *143*, 75–81. [CrossRef]
32. Shakir, R.R.; Zhu, J. Behavior of compacted clay-concrete interface. *Front. Archit. Civ. Eng. China* **2009**, *3*, 85–92. [CrossRef]
33. Liu, J.; Zou, D.; Kong, X. A three-dimensional state-dependent model of soil-structure interface for monotonic and cyclic loadings. *Comput. Geotech.* **2014**, *61*, 166–177. [CrossRef]
34. Chen, X.; Zhang, J.; Xiao, Y.; Li, J. Effect of roughness on shear behavior of red clay-concrete interface in large-scale direct shear tests. *Can. Geotech. J.* **2015**, *52*, 1122–1135. [CrossRef]
35. Hadi, H.; Vahab, S.; Mohammad, F.M.; Ahmadreza, H.; Zheming, Z. Experimental and numerical study of shear fracture in brittle materials with interference of initial double cracks. *Acta Mech. Solida Sin.* **2016**, *29*, 555–566.
36. Di Donna, A.; Ferrari, A.; Laloui, L. Experimental investigations of the soil-concrete interface: Physical mechanisms, cyclic mobilization.; behavior at different temperatures. *Can. Geotech. J.* **2016**, *53*, 659–672. [CrossRef]
37. *ASTM D6913/D6913M-17. Standard Test Methods for Particle-Size Distribution (Gradation) of Soils Using Sieve Analysis*; ASTM International: West Conshohocken, PA, USA, 2017; Available online: https://www.astm.org/Standards/D6913.htm (accessed on 21 September 2020).
38. *ASTM D422-63. Standard Test Method for Particle-Size Analysis of Soils*; ASTM International: West Conshohocken, PA, USA, 2007; Available online: https://www.astm.org/DATABASE.CART/WITHDRAWN/D422.htm (accessed on 21 September 2020).
39. *ASTM D558-11. Standard Test Methods for Moisture-Density (Unit Weight) Relations of Soil-Cement Mixtures*; ASTM International: West Conshohocken, PA, USA, 2011; Available online: https://www.astm.org/Standards/D558.htm (accessed on 2 November 2020).
40. *ASTM D854-14. Standard Test Methods for Specific Gravity of Soil Solids by Water Pycnometer*; ASTM International: West Conshohocken, PA, USA, 2014; Available online: https://www.astm.org/Standards/D854.htm (accessed on 21 September 2020).
41. *ASTM D3080/D3080M-11. Standard Test Method for Direct Shear Test of Soils Under Consolidated Drained Conditions*; ASTM International: West Conshohocken, PA, USA, 2014; Available online: https://www.astm.org/DATABASE.CART/WITHDRAWN/D3080D3080M.htm (accessed on 21 September 2020).
42. Abbas, S.M. *Constitutive Modeling of Rockfill Materials*; Lap Lambert Academic: Saarbrücken, Germany, 2011.
43. Kou, H.L.; Wu, C.Z.; Ni, P.P.; Jang, B.A. Assessment of erosion resistance of biocemented sandy slope subjected to wave actions. *Appl. Ocean Res.* **2020**, *105*, 102401.
44. Dietz, M.S.; Lings, M.L. Postpeak strength of interfaces in a stress-dilatancy framework. *J. Geotech. Geoenviron. Eng.* **2006**, *132*, 1474–1484. [CrossRef]
45. Uesugi, M.; Kishida, H.; Uchikawa, Y. Friction between dry sand and concrete under monotonic and repeated loading. *Soils Found.* **1990**, *30*, 115–128. [CrossRef]

46. Han, F.; Ganju, E.; Salgado, R.; Prezzi, M. Effects of interface roughness, particle geometry, and gradation on the sand-steel interface friction angle. *J. Geotech. Geoenviron. Eng.* **2018**, *144*, 04018096. [CrossRef]